Dedicated to innovation in aerospace

NLR-TP-2021-309 | November 2021

Full process chain simulation of the (wire-based) laser metal deposition process towards fatigue life prediction

CUSTOMER: JU Clean Sky

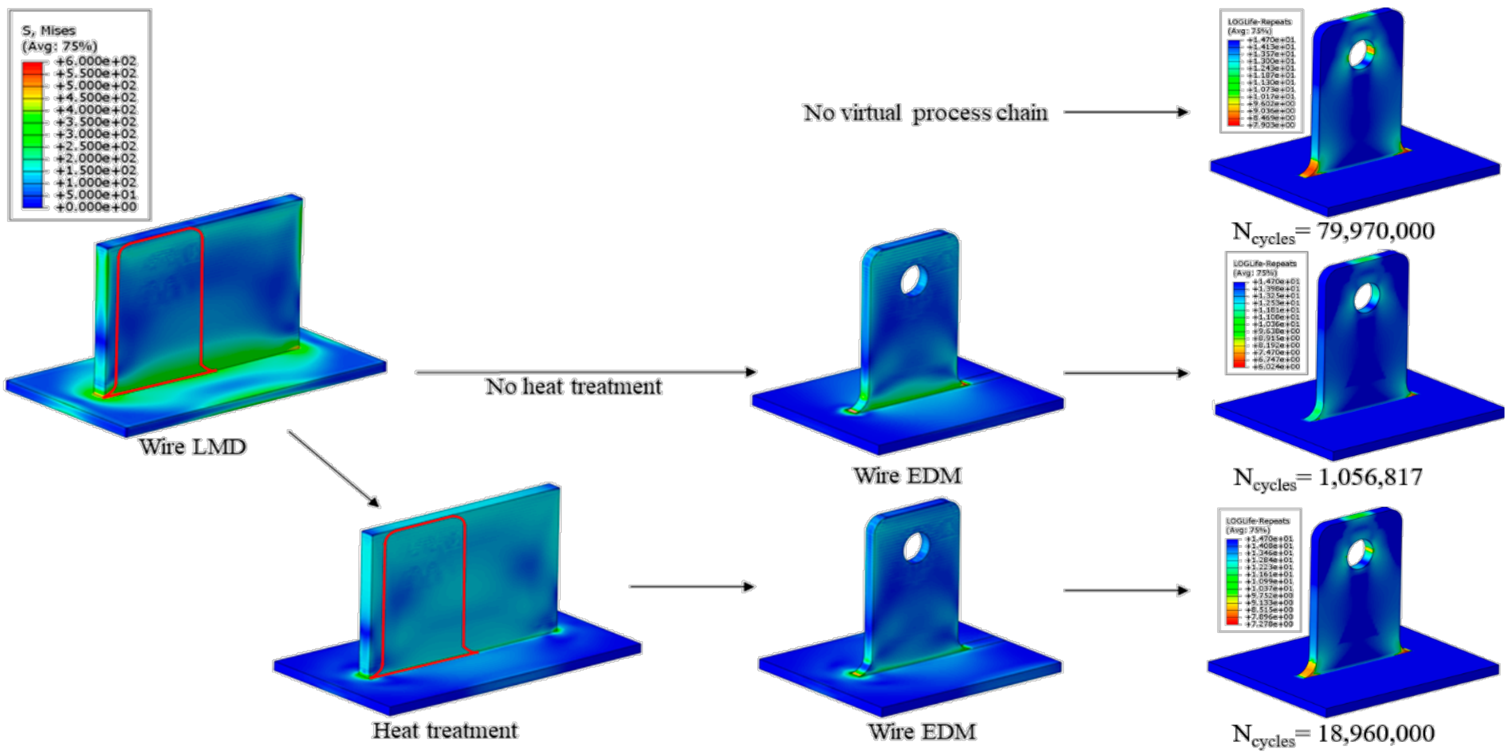

Royal NLR - Netherlands Aerospace Centre

Dedicated to innovation in aerospace

EXECUTIVE SUMMARY

UNCLASSIFIED

Full process chain simulation of the (wire-based) laser metal deposition process towards fatigue life prediction

Problem area

In recent years, metal additive manufacturing (AM) has seen a significant growth in its application in the industry as it enables the manufacturing of complex parts with increased functionalities and lower weight. In the aerospace industry the employment of metal additive manufacturing can have great economic and environmental benefits, as total weight and manufacturing time of aircraft components can be significantly reduced. A critical aspect for parts in the aerospace industry is safety and certification, which is a large obstacle for additive manufactured parts to be incorporated in any aircraft. Related to safety and certification is the fatigue life of the additive manufactured components. Due to the inherent properties of the metal AM process the fatigue life of these parts is often difficult to predict, which is problematic for certification. This study aims to improve the fatigue prediction of AM aircraft fuselage components (complex frame joints) by including the effect of residual stresses using a virtual manufacturing process chain.

Description of work

This report describes the development of a virtual process chain framework for the wire based Laser Metal Deposition process (LMD). The main focus is to determine process induced residual stresses and its influence on the fatigue life of metal AM components. To this end, a low fidelity simulation method for the LMD process is calibrated and validated. Process simulations of the subsequent postprocesses are implemented in a modular fashion and chained with the LMD simulation to obtain the evolution of the process induced residual stress and deformation throughout the process chain.
This virtual process chain is demonstrated on a fictional use-case of a simple bracket. By including the residual stress in a fatigue life prediction of the bracket the (qualitative) influence of different process steps on the fatigue life is investigated.

REPORT NUMBER
NLR-TP-2021-309

AUTHOR(S)
T.P.A. Koenis
W.M. van den Brink
M. Bosman

REPORT CLASSIFICATION
UNCLASSIFIED

DATE
November 2021

KNOWLEDGE AREA(S)
Computational Mechanics and Simulation Technology
Constructie- en fabricagetechnologie

DESCRIPTOR(S)
Virtual Manufacturing
Metal additive manufacturing
Fatigue Life
Process chain

Results and conclusions

The developed virtual process chain can be implemented to obtain estimations of the effect of different process steps on the fatigue life of wire based LMD parts.
The low fidelity method as employed for the analysis of the LMD process was found to sufficiently predict residual stress and deformation for implementation in the virtual process chain. However, further research is required to establish limits for when new calibrations are required.
The modular implementation of subsequent post-processing steps was successful, however further validation of the simulations of individual post-processing steps is required. Since experimental validation has only been performed for the LMD process simulation, the post-processing steps are purely based on literature, and not yet validated experimentally. This validation is critical to ensure that the determined fatigue life is also quantitatively a sound estimation.
To validate the complete virtual process chain and the predicted fatigue life of the manufactured part a comparison of the estimated fatigue life and the actual fatigue life is required.

Applicability

The proposed framework can be used to optimize the process chain as well as individual process steps to maximize the fatigue life of a component manufactured by wire based LMD. As it is a virtual method, this optimization can be performed with minimum material costs as with the “trail-and-error” method.
To better support the certification process of LMD manufactured components in aerospace, the fatigue life prediction should also give quantitatively accurate results. To this end additional validation will be required.
Due to the modular set-up of the framework, validated process simulations of additional or replacing steps can easily be added. Therefore, this method can be easily adjusted to be used for different process chains as well as for completely different fabrication methods.

GENERAL NOTE
This report is based on a presentation held at the ESIAM21, Online, 8-10/09/2021.

Royal NLR
Anthony Fokkerweg 2
1059 CM Amsterdam, The Netherlands
p) +31 88 511 3113
e) info@nlr.nl i) www.nlr.nl

Dedicated to innovation in aerospace

NLR-TP-2021-309 | November 2021

Full process chain simulation of the (wire-based) laser metal deposition process towards fatigue life prediction

CUSTOMER: JU Clean Sky

AUTHOR(S):

T.P.A. Koenis	NLR
W.M. van den Brink	NLR
M. Bosman	GKN Aerospace

Royal NLR - Netherlands Aerospace Centre

This report is based on a presentation held at the ESIAM21 conference, Online, 8-10/09/2021.

The contents of this report may be cited on condition that full credit is given to NLR and the author(s).

This publication has been refereed by the "Advisory Committee Knowledge and Technology."

CUSTOMER	**JU Clean Sky**
CONTRACT NUMBER	**807097, 945583**
OWNER	**NLR + partners**
DIVISION NLR	**Aerospace Vehicles**
DISTRIBUTION	**Unlimited**
CLASSIFICATION OF TITLE	**UNCLASSIFIED**

APPROVED BY:		**Date**
AUTHOR	T.P.A. Koenis	8-11-2021
REVIEWER	E. Amsterdam	8-11-2021
MANAGING DEPARTMENT	A.A. ten Dam	8-11-2021

Summary

As virtual manufacturing in additive manufacturing (AM) becomes more mature, the benefits of using this technology increases. Virtual manufacturing simulations often capture only one step in the AM process chain decoupled from the subsequent steps. However, all steps in the process chain influence the final product in their own way. Therefore, this study focusses on the development of a virtual manufacturing framework to perform sequential process simulations of the complete process chain for AM parts. This framework can ultimately be used to obtain insights on the effect of additional processes or process variations on the final product. In this study, the framework is used to obtain insights on the effect of residual stress due to the laser metal deposition (LMD) process on the fatigue life of the final part. To this end, a calibration and validation of a part-scale LMD process simulation is performed to obtain deformations and residual stresses. This is followed by a heat treatment simulation to determine the effect of post heat treatment on the deformation and residual stresses of the final part. As the numerical simulations of the post-processes are purely based on literature and not validated experimentally, the simulations can only be used to qualitatively estimate the residual stresses after post-processing. By combining the residual stress field with externally applied loads, the effect of different process steps on the fatigue life is investigated. To demonstrate this framework, the full virtual process chain of a fictional use case for a simple aerospace bracket is analyzed to observe qualitatively the influence of individual process steps on the fatigue life of the final component.

Contents

1 Introduction

In recent years, metal additive manufacturing (AM) has seen a significant growth in its application in the industry as it enables the manufacturing of complex parts with increased functionalities and lower weight. In the aerospace industry the employment of metal additive manufacturing can have great economic and environmental benefits, as total weight and manufacturing time of aircraft components can be significantly reduced. A critical aspect for parts in the aerospace industry is safety and certification, which is a large obstacle for additive manufactured parts to be incorporated in any aircraft [1]. Related to safety and certification is the fatigue life prediction during design and fatigue performance during in-service use of aircraft components. This study aims to improve the fatigue prediction of AM aircraft fuselage components (complex frame joints) using a virtual manufacturing process chain.

Due to the characteristics of most metal AM processes, as-build AM parts often contain a large amount of residual stresses, rough outer surfaces and defects [2]. It has been repeatedly shown that these properties of metal AM parts are detrimental for the fatigue behaviour [3, 4, 5]. To this end, metal AM parts are often post-processed by machining and heat treatment to limit the surface roughness, reduce the residual stress and therefore improve the overall fatigue properties [4, 6]. To help with the eventual certification of the complex aerospace metal AM parts, numerical modelling could help with providing insights in process induced effects and improve process control [1]. However, as post-processing of metal AM parts is often required and adds a significant amount of work to the process chain, full process chain simulations could add significant insights on the properties of the final product [7].

Extensive research on process chains for forging, extrusion and other common manufacturing processes has already been performed as reviewed by Afasov [8]. As process simulations of metal AM processes are still maturing, studies on the process chain simulations of metal AM processes are more limited. The handful of studies on AM process chains focus on the laser powder bed fusion (LPBF) process [9, 10, 11]. Afasov et al. [10] expanded the LPBF process chain simulations with fatigue life prediction combining residual stress fields with an S-N curve predictive model. For LMD like metal AM processes, process simulations are less mature and most studies focus on the actual process simulation and not yet the full process chain [12, 13]. Salonitis et al. [7] performed an initial numerical study on multiple process steps in the laser cladding process chain to track the evolution of the process induced residual stresses.

In the current study, the wire based Laser Metal Deposition (LMD) with the titanium alloy Ti-6Al-4V is employed. With this process, a wire is fed towards a printing head containing a laser beam, where the material melts and is deposited in a bead. By moving the printer head, the melt pool is dragged along the substrate to form a track. The first tracks are deposited on a baseplate which is rigidly fixed. By adding track after track in a layer wise manner, a complete 3D part is manufactured. Similarly to other metal AM parts, to implement LMD parts in an aircraft, multiple post processing steps are often required to limit the influence of residual stresses and surface roughness. The LMD process typically has a high surface roughness due to the large deposited bead size as stated by Frazier [14]. Therefore, a machining step is often performed to limit the detrimental effects of the surface roughness. Furthermore, heat treatments are generally employed in the LMD process chain to limit residual stresses and improve part properties.

The aim of this study is to predict the effect of processes in the LMD process chain on the fatigue life of the final aerospace fuselage part and use these predictions to improve this fatigue life. To this end numerical models for simulation of a laser metal deposition process chain have been developed, including the LMD process, the post-heat treatment and wire EDM to obtain the final part. In this study the focus lies on the calibration and validation of a low fidelity and fast simulation approach of the LMD process as well as the chaining of subsequent process simulations to observe process effects on the residual stress of LMD parts.

2 Method

In this study a (wire-based) laser metal deposition (LMD) process chain is investigated using finite element methods. The complete manufacturing process consists of the wire-LMD process followed by a stress-relief heat treatment and a subtractive process to obtain the final part geometry. The subtractive method of wire electrical discharge machining (EDM) is chosen as it has limited effect on surface residual stresses. After manufacturing, the part is subjected to a virtual fatigue test to obtain the fatigue life. Fig. 1 gives a schematic overview of the LMD process chain is studied in this paper, as well as the virtual representation of this process chain, containing all simulation steps.

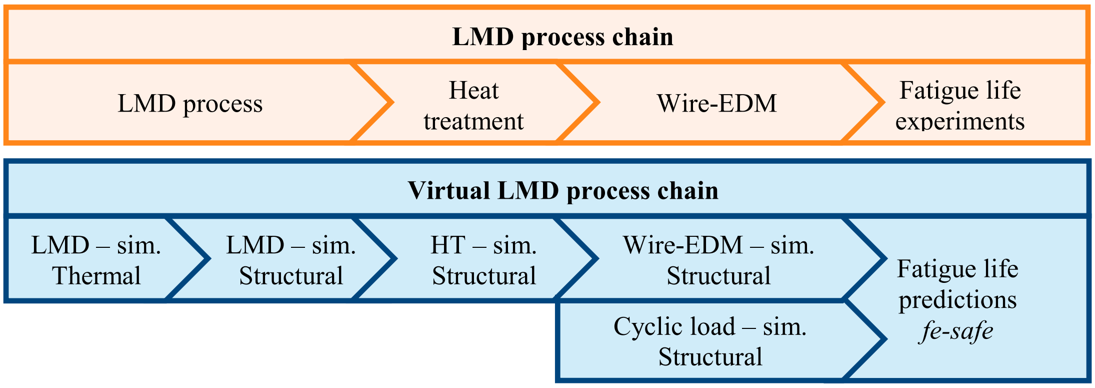

Fig. 1: Schematic overview of the actual LMD and the virtual LMD process chain as implemented in ABAQUS and fe-safe

As stated by Afasov [8], errors of result mapping between different simulation steps accumulate over multiple simulations. Therefore, it is investigated if the different process simulations can be chained directly, without introducing mapping errors. To this end, the output of the sequential models has to be compatible over multiple types of analysis. By incorporating the mesh of the final part throughout the simulation, the same mesh is used for all process steps, and results of subsequent processes can be mapped to exactly the same mesh, limiting errors. All process models have been created within the finite element software *ABAQUS* to avoid mapping between different analysis software. The following subsections will discuss each process simulation step of Fig. 1 individually.

2.1 LMD process simulation

To model the LMD process, a sequential thermo-mechanical model is implemented in *ABAQUS*. To decouple the thermal and structural simulation, it is assumed that the distortions that occur during the LMD process do not significantly influence the temperature field. Both for the thermal and the structural simulations the *ABAQUS* AM Modeler plugin is used. This plugin provides special purpose subroutines and GUI options for including AM related toolpaths for element activation and heat input. Based on the toolpaths and a predefined bead size of 10x1 mm, new elements are activated each time increment.

In the thermal analysis heat is added to newly activated elements based on the laser spot diameter, penetration depth, laser power and absorptivity of the material. Cooling of the part is included via radiation and convection on the outer surfaces. These boundary conditions evolve each increment as new elements are activated. Furthermore, heat is lost through conduction to the fixtures of the baseplate, which is added as an additional boundary condition to the model as used by Chiumenti et al. [12]:

$$q_{conduction} = h_{base}\,(T - T_{base})\,, \tag{1}$$

where k_{base} is the heat transfer coefficient by conduction with the baseplate and T_{base} the temperature of the fixture base equal to room temperature. The thermal parameters, laser absorptivity, emissivity, convection coefficient and conductive heat transfer coefficient depend on a wide range of unknown and varying parameters, these four parameters are to be calibrated to accurately predict the temperature field. The temperature dependent material properties of the Ti-6Al-4V titanium alloy based on Chiumenti et al. [12] are displayed in Fig. 2.

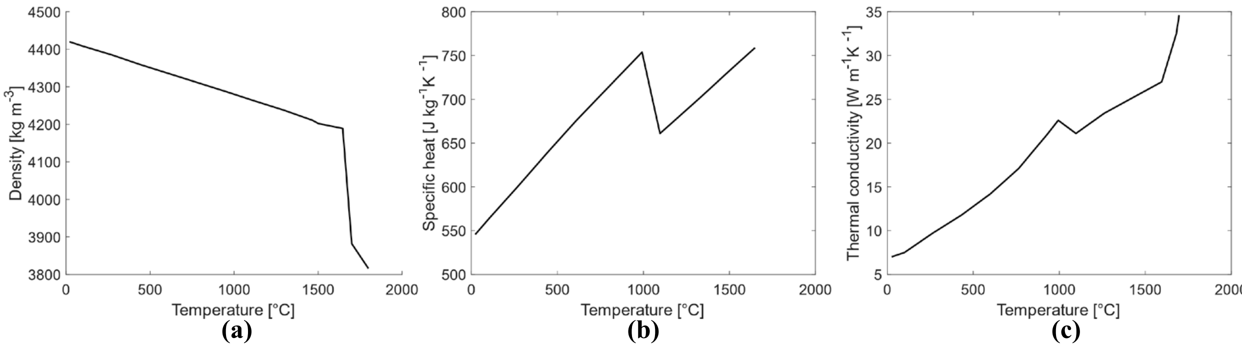

Fig. 2: (a) material density; (b) specific heat; (c) the thermal conductivity Chiumenti et al. [12]

The time incrementation is chosen to correspond with the deposition of a complete track, alternating time increments where a new track is deposited and heat is applied and time increments where the newly deposited track is cooled and no heating is applied. This method is chosen over high fidelity methods to limit the computational cost, which would be large for a full part simulation. By employing the track-by-track method the temperature field obtained from the thermal analysis will not include the local temperature field of the melt pool.
For the structural simulation, elements are activated with the same method as in the thermal simulation. The temperature field obtained in the thermal simulation is added as thermal load in corresponding time increments. Due to the low fidelity simulation approach, the applied thermal load misses information for local temperature fields around the melt pool. To include thermal strains caused by this absent local temperature field, elements are activated using an elevated initial temperature. To determine this initial temperature, a structural calibration is required. In the simulation, the baseplate is clamped corresponding to the employed fixture method. Furthermore, the fixture plate is assumed rigid and frictionless hard contact is defined between the fixture plate and the bottom of the thin baseplate. The temperature dependent material data for the coefficient of thermal expansion (CTE), Youngs modulus and plasticity employed for the structural simulations can be found in Fig. 3.

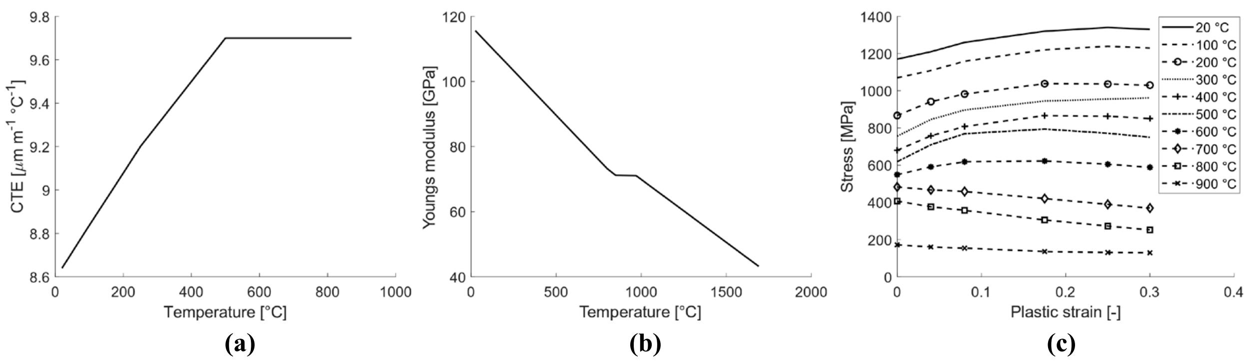

Fig. 3: (a) CTE [15]; (b) Youngs modulus [16]; (c) plasticity curves [17]

Studies by Denlinger et al. [13] and Heigel et al. [15] on directed energy deposition process simulation observed significant effects of stress relaxation during the process due to high temperature creep for the Ti-6Al-4V alloy. Within *ABAQUS*, creep can be incorporated in the model via a the Norton power law,

$$\dot{\epsilon} = A\tilde{q}^n, \tag{2}$$

with $\dot{\epsilon}$ the equivalent creep strain rate, $\tilde{q}$ the uniaxial equivalent deviatoric stress and A and n as material constants to be determined experimentally. Based on Yan et al. [18] and Oliveira et al. [19] an additional Arrhenius term is implemented to obtain the temperature dependent creep law,

$$\dot{\epsilon} = A\tilde{q}^n exp\left(-\frac{Q}{RT}\right) \tag{3}$$

with Q the activation energy, R the universal gas constant and T the absolute temperature in Kelvin. Equation 3 is fitted to experimental data for creep behaviour of the Ti-6Al-4V alloy is obtained from Oliveira et al. [19]. The fitted creep parameters are presented in Table 1.

Table 1: The fit parameters for the temperature dependent creep Norton-Bailey creep law

Calibration parameter	Value	Unit
A	2.36e-3	[MPa^{-n}]
n	6.68	[-]
Q	303e3	[J/mol]
R	8.314	[J/mol K]

2.2 Post treatments simulations

Subsequent to the LMD process, a thermal stress relief treatment and a subtractive process such as machining or wire EDM can be applied. In this study, these post-processing steps will be based purely on literature, as no experimental validation has been performed.
For the post heat treatment analysis three subjects are of interest, namely the thermal analysis, phase changes and structural analysis [20]. Due to the relatively high thermal conductance and thin parts used in this study, it is assumed that the temperature is uniform in the part during the treatment. Therefore, the temperature of the complete part follows the applied temperature cycle and no thermal analysis is required. Furthermore, Yan et al [18] showed that the thermal expansion due to phase change has only a limited influence on the reduction in residual stress in the analysis of heat treatments. Thus, only a structural analysis is employed to model the post heat treatment. The stress relief is modelled using both the temperature dependent plasticity curves as well as temperature dependent Norton creep law, as presented before. For the finite element analysis only a thermal load is applied corresponding to the temperature profile of the actual heat treatment. As the same mesh is used in this analysis as is used for the LMD-process analysis, no mapping of the residual stress field is required as the step is added directly to the LMD analysis. Boundary conditions are only applied to restrict rigid body movements, leaving the part free to deform under the temperature load. Time increments of 500 seconds are applied for this process.
After application of the stress relief treatment, a subtractive processing method is employed to obtain the final shape of the product. In this study it is assumed that the subtractive process employed does not create additional residual stresses. Therefore, to simulate a subtractive processing method, elements outside of the final part geometry can simply be removed from the analysis similarly to Salonitis et al. [7]. The boundary conditions are again applied only to restrict rigid body movements, leaving the new configuration of the part to deform freely.

2.3 Fatigue life predictions

To analyse the influence of the process induced residual stress on the fatigue life of the final product, a fatigue analysis is performed. To this end, the software *fe-safe* is employed to perform a stress based fatigue analysis as it has good interaction with the *ABAQUS* software. Based on the SN-curves, stress field obtained from the cyclic load and a mean stress field due to residual stress the high cycle fatigue life can be estimated. The mean stress field is adopted in *fe-safe* via the Gerber approach. A machined surface with a surface roughness of 4-16 µm is assumed in the fatigue analysis, from which a surface finish correction factor between 1.2 and 1.35. To include effects of process induced porosity on the fatigue life, the SN curve adopted for the deposited material is based on data form Cao et al. [21] where slightly porous Ti-6Al-4V material processed by hydrogen sintering and phase transformation (HSPT) analysed on fatigue life. For the Ti-6Al-4V baseplate, an SN curve is adopted based on wrought material obtained from Cao et al. [21]. Fig. 4 shows the obtained SN curve data together with the power law fit used to implement the SN curve in the fe-safe analysis. To determine the stress field caused by the cyclic load, a structural simulation is performed applying the maximum load. This results in a maximum stress field from which a cyclic load is obtained by cyclically scaling the stress field by -1 to 1. To include process induced residual stress, the obtained residual stress field is added to offset the mean stress field.

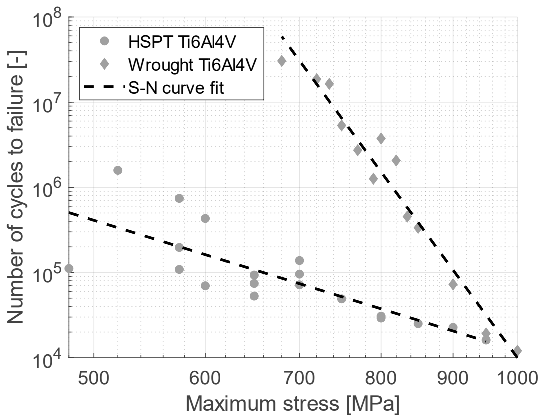

Fig. 4: S-N curve data obtained from Cao et al. [21] for porous hydrogen sintered and wrought Ti-6Al-4V

2.4 LMD model calibration method

To calibrate and verify the thermal and structural models for the LMD process simulations, experimental data is obtained from multiple depositions of a Ti-6Al-4V T-shape. The T-shaped part is approximately 230x100x50 mm and deposited on a thin Ti-6Al-4V baseplate of 500x155x6.35 mm, fixed by evenly spaced bolts along the edge to a steel fixture plate of 512.7x167.7x25.4 mm. This fixture plate is subsequently fixed to an aluminium base block. The layer height of the deposition is approximately 1 mm with a bead with of 10 mm. The deposition is performed using multiple strategies, where strategy 1 employs medium interlayer wait times, strategy 2 longer interlayer wait times and strategy 3 shorter interlayer wait times. All depositions have been performed in a closed, argon atmosphere to prevent oxidation. To calibrate the thermal model, the interlayer temperature is measured at the centre of the newly deposited layer using a pyrometer, where the interlayer temperature is defined as the minimum layer temperature before a new layer is deposited. When the deposition of the part is finished and the material has cooled to room temperature, the baseplate is released from the fixture plate to allow for deformation due to residual stress. The

deformed part and baseplate are 3D scanned to obtain a digital representation of the deformation, which is used to calibrate the structural simulations.
Fig. 5 (a) displays the numerical model created to simulate the T-shape for both the thermal and structural analysis. The finite element model consists of the T-shaped deposition with the baseplate and fixture assembly. The model is meshed with 32,068 8-node linear hexahedral elements of approximately 5x5x1 mm in the T-shape and baseplate. For the steel fixture plate 2,601 10x10x10 mm 8-node linear elements are used. The T-shaped part is sliced in 50 1 mm layers, where each layer is deposited in 2 tracks. Fig. 5 (b) displays the toolpath data of the final layer as obtained from machine log data. Boundary conditions in the thermal analysis are applied as discussed in Section 6. For the structural analysis, elements in a circle of 6 mm around the bolt holes are fixed to simulate the clamping of the bolts. After the LMD process, the fixture plate is removed from the model, as well as the fixed boundary conditions around the bolt holes. Boundary conditions are applied at three corners of the thin baseplate to avoid rigid body motions while allowing for free deformation of the model.

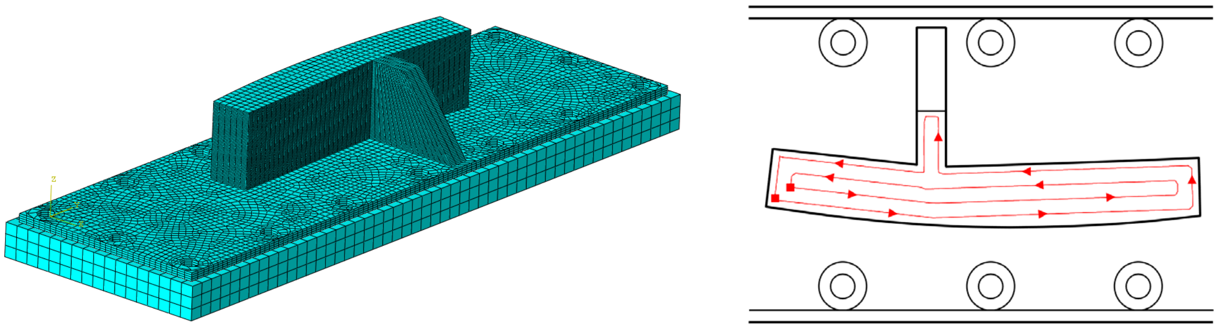

(a) (b)

Fig. 5: (a) finite element (FE) mesh of the T-shaped calibration model; (b) schematic image of the deposition tracks of a single layer

2.5 Case study

To demonstrate the discussed methodology for full process chain simulation, the process chain of a fictional titanium bracket is simulated. This includes the LMD process, heat treatment, removal of elements and a fatigue life estimation. As the simple bracket has not been manufactured, this is purely a numerical exercise to qualitatively evaluate the methodology. The bracket is deposited as a larger wall of 150x100x10 mm, deposited in 50 layers consisting of single tracks. After deposition the part is stress relieved by a post heat treatment at 900 °C for 2 hours. From the stress relieved deposited wall, the bracket is extracted by wire EDM, where it is assumed no additional residual stresses are created. To estimate effects of the process induced residual stress on the fatigue life, the fatigue analysis in *fe-safe* is performed for cyclic loading of the bracket.

Fig. 6 (a) displays the finite element mesh of the titanium deposition and fixture assembly consisting of 73,508 hex elements, from which the titanium bracket is extracted. Fig. 6 (b) displays the mesh of the final bracket geometry extracted from the deposited wall. The LMD process is modelled in a similar fashion as the T-shaped part, adopting calibrated thermal parameters in the thermal analysis and the calibrated initial temperature in the structural analysis. In the thermal LMD analysis, the same boundary conditions are employed as for the T-shape. In the structural LMD analysis the fixed bolt boundary conditions are replaced for a clamping boundary along the edge of the baseplate. After the LMD analysis, the results are used in the heat treatment analysis, where the plate is allowed to deform freely, employing boundary conditions to avoid rigid body motions. The temperature profile is added as a

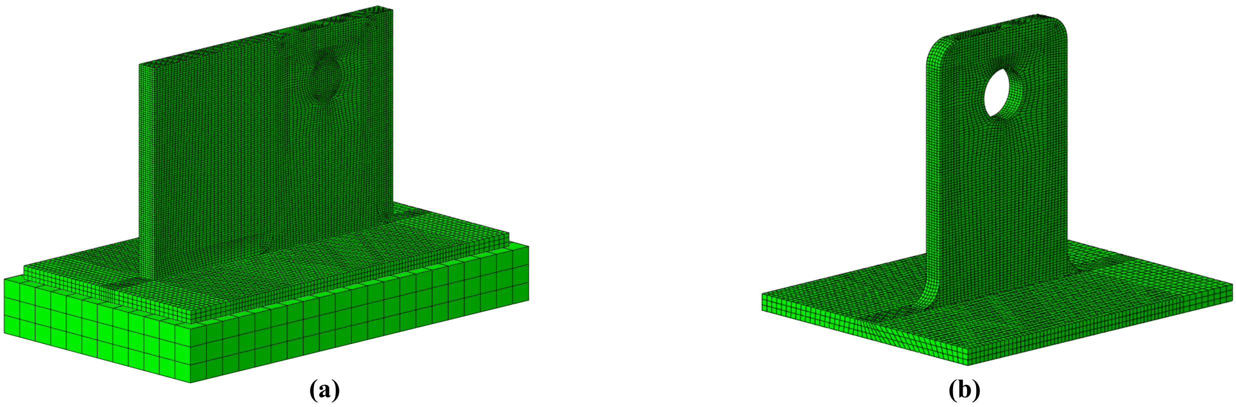

Fig. 6: a) FE mesh for the LMD process simulation; (b) the FE mesh of the final bracket design extracted from the original mesh

homogeneous load to all nodes in the model under the assumption that the thin parts heat up homogeneously. After the heat treatment analysis, the elements outside of the bracket geometry are removed and boundary conditions to avoid rigid body motion are reapplied.

To obtain the cyclic stress field as employed in the fatigue analysis, the loading is simulated without the residual stress and strain from the process simulations. In this analysis, the model is clamped along the edge of the baseplate, and a load of 5 kN is applied at the hole in the deposited bracket. The stress field obtained from this analysis is imported in the fatigue life analysis using scaling from 1 to -1 of the stress values to obtain a cyclic stress field. Multiple fatigue life analyses have been performed adopting different means stress fields. The first analysis is without any residual stress, and thus a mean stress of 0. To observe the effect of the LMD process chain on the fatigue life, the residual stress field obtained after wire EDM is adopted in a second fatigue life analysis. Finally the residual stress field is obtained when heat treatment is not included in the virtual process chain. This residual stress field is adopted in a third fatigue life analysis to observe the effects of heat treatment on the fatigue life of a LMD manufactured part.

3 Results and discussion

3.1 LMD process simulation calibration and validation

Fig. 7 a displays the measured interlayer temperature over the normalized manufacturing time of the T-shaped part deposited with strategy 1, which is used to calibrate the thermal model. To calibrate the thermal model, the laser absorptivity, emissivity, convection coefficient and conductive heat transfer coefficient are varied to match the trend and temperature values obtained experimentally. The calibrated thermal parameters are displayed in Table 2. When comparing these parameters with parameters observed in literature, it is observed that they are in a realistic range [12, 22]. These parameters have been employed to model the use of strategy 2 and strategy 3 to verify the thermal modelling method. Fig. 7 b shows the comparison between the experimental and numerical interlayer temperatures over the normalized manufacturing time for both strategies. As can be observed in this figure, the experimental results are less consistent compared to the calibration experiment, as multiple breaks were required to correctly manufacture the parts. However, these breaks are captured in the machine log data and thus can be implemented in the numerical simulations. The simulations generally show good correspondence with the experimental data, which is sufficient to implement the temperature results in the mechanical simulation.

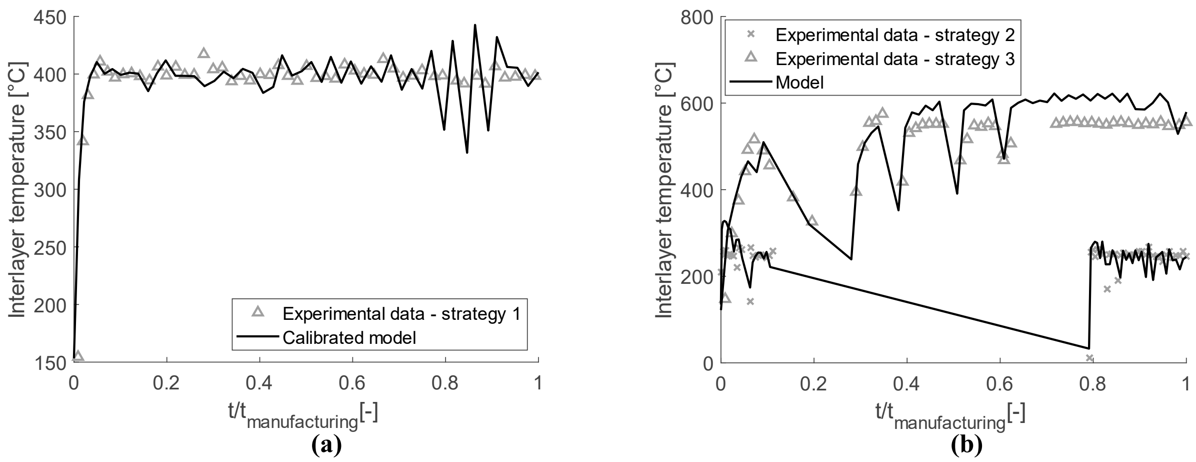

Fig. 7: (a) interlayer temperature profile for model calibration; (b) interlayer temperature profiles for model validation

Fig. 8 (a) illustrates the extraction of the plate deformation to use in the mechanical calibration from the 3D scans of the deformed baseplate and deposition. The coordinates of the nodes located near the edge indicated by the red arrow and line in Fig. 8 (a) have been extracted for all three manufacturing strategies. These coordinates are displayed in 2D in Fig. 8 (b) to illustrate the deformation profile along this edge. From the numerical simulation of the T-shape manufactured with strategy 1, the same deformation profile has been extracted to compare with the experimental results. By varying the initial temperature at which elements are activated, the mechanical model has been calibrated to match the deformation profile for strategy 1. The initial temperature is calibrated to a value of 550 °C. Similarly to the thermal analysis, the structural analysis is validated using the experimental results of the T-shapes manufactured with strategy 2 and 3. This comparison is illustrated in the same graph of Fig. 8 (b). Slight differences in deformation profile are observed for both strategies. However, the overall amount of deflection in the baseplate predicted by the calibrated model corresponds well with the deflection obtained experimentally. This indicates that the residual stresses introduced by the LMD process are captured well by the calibrated model. It should be mentioned that there are limitations to the applicability of the model. For example significantly different set-ups in fixture assembly, or too large deformations of the baseplate during the LMD process could strongly change the heat loss through conduction. Therefore, further research would be required with different geometries and fixture assemblies to obtain an indication when recalibration of the calibration parameters is required.

Table 2: The calibrated parameters for both the thermal and structural LMD process simulations

Calibration parameter	Value	Unit
Absorptivity	0.675	[-]
Emissivity	0.8	[-]
Convection coefficient	35	[W/m^{2}K]
Heat transfer coefficient for conduction	2.5	[W/m^{2}K]
Initial temperature	550	[°C]

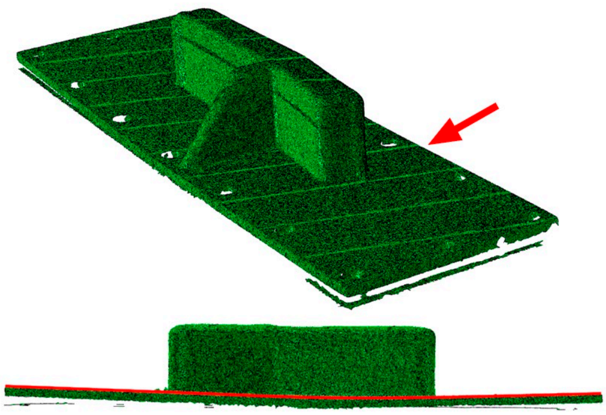

(a)

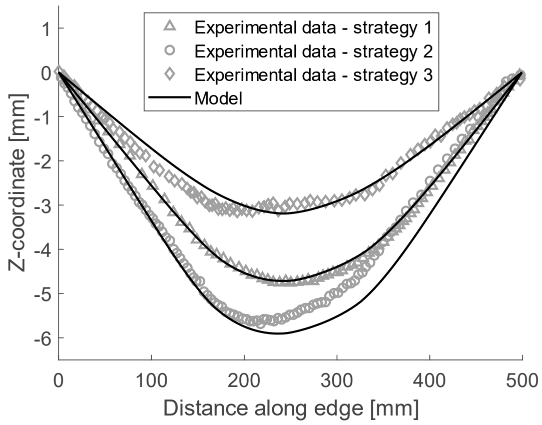

(b)

Fig. 8: (a) location of deformation profile extracted from the 3D scans; (b) deformation profiles for model calibration and validation

3.2 Case study

Fig. 9 displays the residual stress field evolution throughout the different virtual process chains, with the location of the bracket in the deposited wall indicated by red contours. After the LMD process, the highest residual stresses are observed at the interface with the baseplate of the deposited wall and at the top layers, which corresponds well with observations from literature [23]. If a subsequent heat treatment is performed, the stress concentrations are reduced, and the residual stress field becomes more homogeneous. However, the deposited material still contains increased stress at the connection with the baseplate. These stress concentrations are more pronounced after the wire EDM process step.

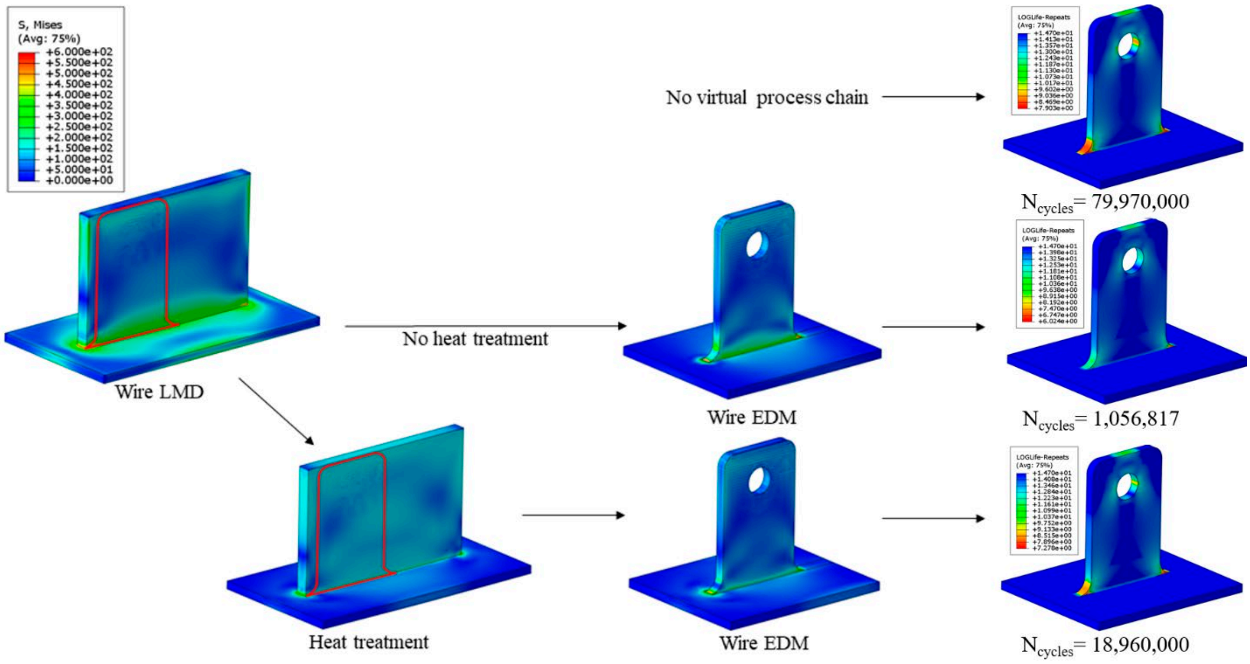

Fig. 9: Evolution of the process induced residual stress field for different process chains obtained by the process chain simulations

The effect of the process induced residual stress is most visible in the fatigue analysis results. Without residual stress, a number of cycles to failure of 79,970,000 was observed. However, if the residual stress of the process chain without heat treatment is included, the number of cycles to failure drops with almost 98.7% to 1,056,817. This corresponds qualitatively with the expectations, as the tensile residual stresses after the LMD process are significant. As expected in literature, significant amount of cycles to failure is recovered by including the heat treatment in the virtual process chain [6]. With 18,960,000 cycles to failure the fatigue life is reduced by a factor of 4 compared to the reference case with no residual stress, which is more than 17 times the estimated fatigue life of the bracket without heat treatment. It can be stated that qualitatively this fast virtual LMD process chain simulation approach corresponds with the expectations. However, before this method can be employed to optimize the process steps for fatigue life of aerospace components, more validation is required. To obtain quantitatively correct estimations of the fatigue life of LMD manufactured parts, the model as used for the heat treatment has to be verified as performed for other alloys in similar studies [9, 11]. Furthermore, implementation of different postprocessing steps, e.g. machining or shot-peening can have significant effects on the surface roughness and residual stress thus influencing the fatigue life of the components as observed by Afazof et al. [10]. Finally, the adopted SN-curves for the fatigue life analysis are highly dependable on the size and type of porosity in the material. Therefore the actual SN-curve of the material could vary from location to location in the additively manufactured part. The virtual process chain towards fatigue analysis could be further validated by performing fatigue tests on LMD manufactured components with and without post heat treatment and machining.

The method of using the same mesh throughout the virtual process chain to avoid mapping was observed to work well for simple geometries such as the bracket as used in the case study. However, when more complex geometries are involved, it might become more challenging to include the final part in the original mesh for the LMD process simulations, requiring finer elements. In this case, mapping of the stresses from one mesh to the other might be preferable to reduce computational costs. Similarly, remeshing and mapping might be required when deformations become so severe that the result after machining does not correspond with the desired final part.

4 Conclusions

In this paper, the simulation of the complete metal additive manufacturing LMD process chain towards fatigue life estimation has been demonstrated. In the aerospace industry the use of metal additive manufacturing can have great economic and environmental benefits, as total weight, waste and manufacturing time of aircraft components can be significantly reduced. However static and fatigue performance needs to be maintained. It can be stated that qualitatively the presented fast virtual LMD process chain simulation approach corresponds with the expectations. The following conclusions can be made from the current results:

The low fidelity method as employed to analyze the LMD process without large computational cost was found to sufficiently predict residual stress and deformation for implementation in the virtual process chain. However, further research is required to establish limits for when new calibrations are required.

The current method for analyzing the effects of the LMD process chain on the fatigue life of the final product was found to give qualitatively good results. Further validation of individual post-processing steps is required to ensure that the obtained fatigue life is also quantitatively a sound estimation.

The implementation of direct chaining of the virtual process simulations without introducing mapping and mapping errors was observed to work well for simple geometries and low deformations. For complex geometries mapping errors will be more difficult to avoid.

Future work is to improve the fatigue prediction and optimize the process steps for increased fatigue life of AM aircraft fuselage components (complex frame joints). To achieve this more validation is required.

5 Acknowledgements

This project has received funding from the Clean Sky 2 Joint Undertaking (JU) under grant agreement No 945583. The JU receives support from the European Union’s Horizon 2020 research and innovation programme and the Clean Sky 2 JU members other than the Union.

Disclaimer

The results, opinions, conclusions, etc. presented in this work are those of the author(s) only and do not necessarily represent the position of the JU; the JU is not responsible for any use made of the information contained herein.

References

[1] A. Uriondo, M. E. Miguez and S. Perinpanayagam, “The presnet and future of additive manufacturing in the aerospace sector: A review of important aspects,” *Journal of Aerospace Engineering,* vol. 229, pp. 1-16, 2015.

[2] A. Yadollahi and N. Shamsaei, “Additive Manufacturing of Fatigue Resisitant Materials: Challenges and Oppertunities,” *International Journal of Fatigue,* vol. 98, pp. 14-31, 2017.

[3] A. Sterling, B. Torries, N. Shamsaei, S. Thompson and D. Seely, “Fatigue Behavior and Failure Mechanisms of Direct Laser Deposited Ti-6Al-4V,” *Materials Science and Engineering,* vol. 655, pp. 100-112, 2016.

[4] E. Wycisk, A. Solbach, S. Siddique, D. Herzog, F. Walther and C. Emmelmann, “Effects of Defects in Laser Additive Manufactured Ti6Al4V on Fatigue Properties,” *Physics Procedia,* vol. 56, pp. 371-378, 2014.

[5] P. Edwards and M. Ramulu, “Fatigue performance evaluation of selective laser melted Ti-6Al-4V,” *Materials Science and Engineering,* vol. 598, pp. 327-337, 2014.

[6] A. Yadollahi, N. Shamsaei, S. M. Thompson, A. Elwany and L. Bian, “Effects of building orientation and heat treatment on fatigue behavior of selective laser melted 17-4 PH stainless steel,” *International Journal of Fatigue,* vol. 94, pp. 218-235, 2017.

[7] K. Salonitis, L. D'Alvise, B. Schoinochoritis and D. Chantzis, “Additive manufacturing and post-processing simulation: cladding followed by high speed machining,” *International Journal of Advanced Manufacture Technology,* vol. 85, pp. 2401-2411, 2016.

[8] S. M. Afasov, “Modelling and simulation of manufacturing process chains,” *CIRP Journal of Manufacturing Science and Technology,* vol. 6, pp. 70-77, 2013.

[9] D. De Baere, M. Moshiri, S. Mohanty, G. Tosello and J. H. Hattel, “Numerical Investigation into the Effect of Different Parameter on the Geometrical Precision in the LAser-Based Powder Bed Fusion Process Chain,” *Applied Sciences,* vol. 10, p. 3414, 2020.

[10] S. Afazof, J. Frame, U. Ankalkhope, P. Bidare, Y. Liu, W. Vesga and B. Dutton, “Prediction of Residual Stress Evolution for End-To-End Process Chain of Laser Powder Bed Fusion Process and Determination of Fatigue S-N Curves,” in *Structural Integrity of Additive Manufactured Materials and Parts*, West Conshohocken, 2020.

[11] J. M. O'Brien, S. Montgomery, A. Yaghi and S. M. Afasov, “Process chain simulation of laser powder bed fusion including heat treatment and surface hardening,” *CIRP Journal of Manufacturing Science and Technology,* vol. 32, pp. 266-276, 2021.

[12] M. Chiumenti, X. Lin, M. Cervera, W. Lei, Y. Zheng and W. Huang, “Numerical simulation and experimental calibration of Additive Manufacturing by blown powder technology. Part I: thermal anaysis,” *Rapid Prototyping Journal,* vol. 23, pp. 448-463, 2017.

[13] E. R. Denlinger, J. C. Heigel and P. Michaleris, “Residual stress and distortion modeling of electron beam direct manufacturing Ti-6Al-4V,” *Journal of Engineering Manufacture,* vol. 229, pp. 1803-1813, 2014.

[14] W. Frazier, “Metal Additive Manufacturing: A Review,” *Journal of Materials Engineering and Performance,* vol. 23, pp. 1917-1928, 2014.

[15] J. C. Heigel, P. Michaleris and E. W. Reutzel, “Thermo-mechanical model development and validation of directed energy deposition additive manufacturing of Ti-6A;-4V,” *Additive Manufacturing,* vol. 5, pp. 9-19, 2015.

[16] T. Spittel and M. Spittel, Part 2: Non-ferrous Alloys - Light Metals, Berlin: Heidelberg, 2011.

[17] E. Doege, H. Meyer-Nolkemper and I. Saeed, Fließkurvenatlas metallischer Werkstoffe: Mit Fließkurven für 73 Werkstoffe und einer grundlegenden Einführung, München: Hanser, 1986.

[18] G. Yan, A. Grivoi, Y. Sun, N. Maharjan, X. Song, F. Li and M. J. Tan, “An Arrhenius equation-based model to predict the residual stress relief of post weld heat treatment of Ti-6Al-4V plate,” *Journal of Manufacturing Processes,* vol. 32, pp. 763-772, 2018.

[19] V. M. Oliveira, M. C. da Silva, C. G. Pinto, P. A. Suzuki, J. P. Machado, V. M. Chad and M. J. Barboza, “Short-term creep properties of Ti-6Al-4V alloy subjected to surface plasma carburizing process,” *Journal of Materials Research and Technology,* vol. 4, pp. 359-366, 2015.

[20] J. Rohde and A. Jeppsson, “Literature review of heat treatment simulations with repsect to phase transformation, residual stresses and distortion,” *Scandinavian Journal of Metallurgy,* vol. 29, pp. 47-62, 2000.

[21] F. Cao and K. Ravi Chandran, "The role of crack origin size and early stage crack growth on high cycle fatigue of powder metallurgy Ti-6Al-4V," *International Journal of Fatigue,* vol. 102, pp. 48-58, 2017.

[22] J. Ye, A. Rubenchik, M. F. Crumb, G. Guss and M. Matthews, "Laser Asorption and Scaling Behavior in Powder Bed Fusion Additive Manufacturing of Metals," in *2018 Conerence on Lasers and Electro-Optics (CLEO)*, 2018.

[23] B. Schoinochoritis, D. Chantzis and K. Salonitis, "Simulation of metallic powder bed additive manufacturing processes with the finite element method: A critical review," *Journal of Engineering Manufacture,* vol. 231, pp. 96-117, 2015.

Dedicated to innovation in aerospace

Royal NLR - Netherlands Aerospace Centre

NLR operates as an objective and independent research centre, working with its partners towards a better world tomorrow. As part of that, NLR offers innovative solutions and technical expertise, creating a strong competitive position for the commercial sector.

NLR has been a centre of expertise for over a century now, with a deep-seated desire to keep innovating. It is an organisation that works to achieve sustainable, safe, efficient and effective aerospace operations.
The combination of in-depth insights into customers' needs, multidisciplinary expertise and state-of-the-art research facilities makes rapid innovation possible. Both domestically and abroad, NLR plays a pivotal role between science, the commercial sector and governmental authorities, bridging the gap between fundamental research and practical applications. Additionally, NLR is one of the large technological institutes (GTIs) that have been collaborating over a decade in the Netherlands on applied research united in the TO2 federation.

From its main offices in Amsterdam and Marknesse plus two satellite offices, NLR helps to create a safe and sustainable society. It works with partners on numerous programmes in both civil aviation and defence, including work on complex composite structures for commercial aircraft and on goal-oriented use of the F-35 fighter. Additionally, NLR helps to achieve both Dutch and European goals and climate objectives in line with the Luchtvaartnota (Aviation Policy Document), the European Green Deal and Flightpath 2050, and by participating in programs such as Clean Sky and SESAR.

For more information visit: **www.nlr.org**

Postal address
PO Box 90502
1006 BM Amsterdam, The Netherlands
e) info@nlr.nl i) www.nlr.org

Royal NLR
Anthony Fokkerweg 2
1059 CM Amsterdam, The Netherlands
p) +31 88 511 3113

Voorsterweg 31
8316 PR Marknesse, The Netherlands
p) +31 88 511 4444